

# The ASAS-SN Catalog of Variable Stars III: *Variables in the Southern TESS Continuous Viewing Zone*

T. Jayasinghe<sup>1,2</sup>\*, K. Z. Stanek<sup>1,2</sup>, C. S. Kochanek<sup>1,2</sup>, B. J. Shappee<sup>3</sup>,  
 T. W. -S. Holoienc<sup>4</sup>, Todd A. Thompson<sup>1,2,5</sup>, J. L. Prieto<sup>6,7</sup>, Subo Dong<sup>8</sup>, M. Pawlak<sup>9</sup>,  
 O. Pejcha<sup>9</sup>, J. V. Shields<sup>1</sup>, G. Pojmanski<sup>10</sup>, S. Otero<sup>11</sup>, N. Hurst<sup>12</sup>, C. A. Britt<sup>12</sup>,  
 D. Will<sup>1,12</sup>

<sup>1</sup>Department of Astronomy, The Ohio State University, 140 West 18th Avenue, Columbus, OH 43210, USA

<sup>2</sup>Center for Cosmology and Astroparticle Physics, The Ohio State University, 191 W. Woodruff Avenue, Columbus, OH 43210, USA

<sup>3</sup>Institute for Astronomy, University of Hawaii, 2680 Woodlawn Drive, Honolulu, HI 96822, USA

<sup>4</sup>Carnegie Observatories, 813 Santa Barbara Street, Pasadena, CA 91101, USA

<sup>5</sup>Institute for Advanced Study, Princeton, NJ, 08540

<sup>6</sup>Núcleo de Astronomía de la Facultad de Ingeniería y Ciencias, Universidad Diego Portales, Av. Ejército 441, Santiago, Chile

<sup>7</sup>Millennium Institute of Astrophysics, Santiago, Chile

<sup>8</sup>Kavli Institute for Astronomy and Astrophysics, Peking University, Yi He Yuan Road 5, Hai Dian District, China

<sup>9</sup>Institute of Theoretical Physics, Faculty of Mathematics and Physics, Charles University in Prague, Czech Republic

<sup>10</sup>Warsaw University Observatory, Al Ujazdowskie 4, 00-478 Warsaw, Poland

<sup>11</sup>The American Association of Variable Star Observers, 49 Bay State Road, Cambridge, MA 02138, USA

<sup>12</sup>ASC Technology Services, 433 Mendenhall Laboratory 125 South Oval Mall Columbus OH, 43210, USA

Accepted XXX. Received YYY; in original form ZZZ

## ABSTRACT

The All-Sky Automated Survey for Supernovae (ASAS-SN) provides long baseline ( $\sim 4$  yrs) light curves for sources brighter than  $V \lesssim 17$  mag across the whole sky. The Transiting Exoplanet Survey Satellite (TESS) has started to produce high-quality light curves with a baseline of at least 27 days, eventually for most of the sky. The combination of ASAS-SN and TESS light curves probes both long and short term variability in great detail, especially towards the TESS continuous viewing zones (CVZ) at the ecliptic poles. We have produced  $\sim 1.3$  million V-band light curves covering a total of  $\sim 1000 \text{ deg}^2$  towards the southern TESS CVZ and have systematically searched these sources for variability. We have identified  $\sim 11,700$  variables, including  $\sim 7,000$  new discoveries. The light curves and characteristics of the variables are all available through the ASAS-SN variable stars database (<https://asas-sn.osu.edu/variables>). We also introduce an online resource to obtain pre-computed ASAS-SN V-band light curves (<https://asas-sn.osu.edu/photometry>) starting with the light curves of the  $\sim 1.3$  million sources studied in this work. This effort will be extended to provide ASAS-SN light curves for  $\sim 50$  million sources over the entire sky.

**Key words:** stars:variables – stars:binaries:eclipsing – catalogues – surveys

## 1 INTRODUCTION

The study of stellar variability has been invigorated by the advent of modern large scale sky surveys in the modern era. Recent surveys such as the All-Sky Automated Survey (ASAS; Pojmanski 2002), the Optical Gravitational Lensing Experiment (OGLE; Udalski 2003), the Northern Sky Variability Survey (NSVS; Woźniak et al. 2004), MACHO (Al-

cock et al. 1997), EROS (Derue et al. 2002), the Catalina Real-Time Transient Survey (CRTS; Drake et al. 2014), the Asteroid Terrestrial-impact Last Alert System (ATLAS; Tonry et al. 2018; Heinze et al. 2018), and Gaia (Gaia Collaboration et al. 2018a; Holl et al. 2018; Gaia Collaboration et al. 2018b) have collectively discovered  $\gtrsim 10^6$  variables.

Variable stars are excellent astrophysical probes and have been used in numerous astronomical contexts. Pulsating variables such as Cepheids and RR Lyrae stars are commonly used as distance indicators owing to the period

\* E-mail: jayasinghe@archchilage.1@osu.edu

luminosity relationships seen amongst these variables (e.g., Leavitt 1908; Matsunaga et al. 2006; Beaton et al. 2018, and references therein). Eclipsing binary stars are excellent probes of stellar systems and with sufficient radial velocity followup, allow for the derivation of useful astrophysical parameters, including the masses and radii, of the stars in these systems (Torres et al. 2010). Variable stars are also useful for the study of stellar populations and Galactic structure (Matsunaga 2018; Feast, & Whitelock 2014).

Until recently, the All-Sky Automated Survey for Supernovae (ASAS-SN, Shappee et al. 2014; Kochanek et al. 2017) monitored the visible sky to a depth of  $V \lesssim 17$  mag with a cadence of 2–3 days using two units in Chile and Hawaii each with 4 telescopes. Starting in 2017, ASAS-SN expanded to 5 units with 20 telescopes. The 3 new units all started with g-band filters and the 2 original units have now switched to g-band as well. The ASAS-SN telescopes are hosted by the Las Cumbres Observatory (LCO; Brown et al. 2013) in Hawaii, Chile, Texas and South Africa. ASAS-SN primarily focuses on the detection of bright supernovae (e.g., Holoi en et al. 2017, 2018a), tidal disruption events (e.g., Holoi en et al. 2014, 2016, 2018b) and other transients (e.g., Tucker et al. 2018; Rodríguez et al. 2018), but its excellent baseline allows for the study of variability amongst the  $\gtrsim 50$  million bright ( $V < 17$  mag) sources across the whole sky. ASAS-SN team members have also studied the relative specific Type Ia supernovae rates (Brown et al. 2018) and the largest amplitude M-dwarf flares seen in ASAS-SN (Schmidt et al. 2018).

In Paper I (Jayasinghe et al. 2018a), we reported  $\sim 66,000$  new variables that were flagged during the search for supernovae, most of which are located in regions close to the Galactic plane or Celestial poles which were not well-sampled by previous surveys. In Paper II (Jayasinghe et al. 2018b), we uniformly analyzed  $\sim 412,000$  known variables from the VSX catalog, and developed a robust variability classifier utilizing the ASAS-SN V-band light curves and data from external catalogues. We have also explored the synergy between ASAS-SN and APOGEE (Holtzman et al. 2015) with the discovery of the first likely non-interacting binary composed of a black hole with a field red giant (Thompson et al. 2018) and a detailed variability analysis of the APOGEE sources to identify 1914 periodic variables (Pawlak et al., in prep.). We have also identified rare variables, including 2 very long period detached eclipsing binaries (Jayasinghe et al. 2018c,d) and 19 R Coronae Borealis stars (Shields et al. 2018).

The Transiting Exoplanet Survey Satellite (TESS; Ricker et al. 2015) will produce a large number of high-quality light curves with a baseline of at least 27 days for most of the sky. The TESS input catalog (TIC; Stassun et al. 2018) contains  $\sim 470$  million sources, out of which 200,000 selected targets are observed at a 2 min cadence, while the remaining sources are observed with a cadence of 30 min. Oelkers et al. (2018) recently identified variable sources in a sample of 4 million TIC sources, but did not classify these variables into explicit types. These sources were classified in paper II using ASAS-SN data.

Sources closer to the TESS continuous viewing zone (CVZ) will be observed for a substantially longer period, approaching one year and  $\sim 15,000$  epochs at the ecliptic poles. These TESS light curves will probe short period variability in great detail. ASAS-SN provides long baseline ( $\gtrsim 4$  yr) light

curves sampled at a cadence of  $\sim 1$ –3 days, that complement the TESS light curves.

We extracted the ASAS-SN light curves of  $\sim 1.3$  million sources within 18 deg of the Southern Ecliptic Pole. These sources are within the Southern TESS CVZ and will have well-sampled TESS light curves. In this work, we systematically search this sample for variable sources. This is, in part, a test run for carrying out such a search over the entire sky. In Section §2, we discuss the ASAS-SN observations and data reduction procedures. Section §3 discusses the variability search and classification procedures. In Section §4, we discuss our results and present a summary of our work in Section §5. All the light curves of these sources are made available to the public through our online database.

## 2 OBSERVATIONS AND DATA REDUCTION

We started with the AAVSO Photometric All-Sky Survey (APASS; Henden et al. 2015) DR9 catalog as our input source catalog. We selected all the APASS sources with  $V < 17$  mag in all the ASAS-SN fields with central field coordinates within 18 deg from the Southern Ecliptic Pole ( $\alpha = 90$  deg,  $\delta = -66.55$  deg). This resulted in a list of  $\sim 1.3$  M sources spanning a total of  $\sim 1,000$  deg $^2$ . ASAS-SN V-band observations were made by the “Brutus” (Haleakala, Hawaii) and “Cassius” (CTIO, Chile) quadruple telescopes between 2013 and 2018. Each ASAS-SN field has  $\sim 200$ –600 epochs of observation to a depth of  $V \lesssim 17$  mag. Each camera has a field of view of 4.5 deg $^2$ , the pixel scale is 8''.0 and the FWHM is  $\sim 2$  pixels. ASAS-SN nominally saturates at  $\sim 10$ –11 mag, but light curves of saturated sources are sometimes quite good due to corrections made for bleed trails (see Kochanek et al. 2017).

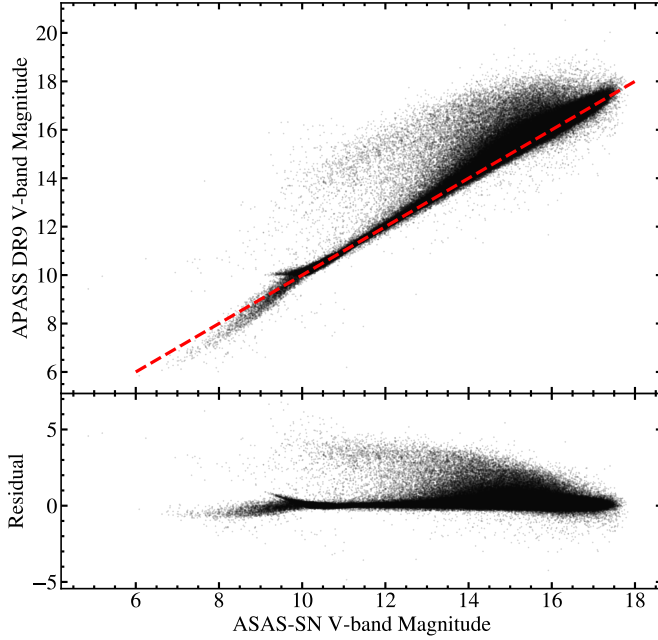
The light curves for these sources were extracted as described in Jayasinghe et al. (2018a) using image subtraction (Alard & Lupton 1998; Alard 2000) and aperture photometry on the subtracted images with a 2 pixel radius aperture. The APASS catalog was used for calibration. The zero point offsets between the different cameras were corrected as described in Jayasinghe et al. (2018a).

Figure 1 illustrates the relationship between the measured mean ASAS-SN V-band magnitudes and the APASS DR9 V-band magnitudes. Sources with  $V_{\text{mean}} \lesssim 14$  mag have similar V-band magnitudes, but a large fraction of the sources with  $V_{\text{mean}} \gtrsim 14$  mag show a discrepancy between the ASAS-SN and APASS measurements. This is due to blending in fields with significant stellar densities (i.e., the LMC in this work). The relatively large ASAS-SN pixel scale of 8''.0 as compared to the smaller APASS pixel scale of 2''.6 makes ASAS-SN photometry more susceptible to blending. Thus, ASAS-SN V-band measurements are systematically brighter for most sources in the LMC due to blended light.

The light curve extraction provides a statistical error estimate, but the scatter in the light curves of apparently non-variable sources is generally larger than expected given the nominal statistical uncertainties. In Jayasinghe et al. (2018a), we used the reduced  $\chi^2$  statistic,

$$\frac{\chi^2}{N_{\text{DOF}}} = \frac{1}{N-1} \sum_{i=1}^N \left( \frac{V_i - V_{\text{mean}}}{\sigma(V_{\text{mean}})} \right)^2 \approx 1, \quad (1)$$

where  $V_i$  is the V-band magnitude for epoch  $i$ , and  $V_{\text{mean}}$



**Figure 1.** Comparison of the mean ASAS-SN V-band magnitudes to the APASS DR9 V-band magnitudes. The red dashed line illustrates a perfect calibration.

is the mean V-band magnitude to determine the typical total uncertainty  $\sigma(V_{\text{mean}})$  as a function of magnitude. In this work, we update our approach to estimating the systematic uncertainties in the ASAS-SN photometry.

We can view the photometric errors as the quadrature sum of the estimated statistical uncertainty  $\sigma_{\text{stat}}$  and a systematic  $\sigma_{\text{sys}}$ , with

$$\sigma^2 = \sigma_{\text{sys}}^2 + \sigma_{\text{stat}}^2. \quad (2)$$

We can measure  $\sigma$  as the root-mean-square (rms) scatter in the light curves of non-variable stars, and then subtract the estimated statistical errors to derive  $\sigma_{\text{sys}}$ , with the results shown in Figure 2 for the 1.3M sources in our sample. For sources with  $V_{\text{mean}} < 13$  mag, the photometric uncertainties approach an ASAS-SN error floor of  $\sim 0.02$  mag. For the sources with  $V_{\text{mean}} > 13$  mag, we fit a third order polynomial,

$$\log \sigma_{\text{sys}} = A(x - 13)^3 + B(x - 13)^2 + C(x - 13) - 1.738, \quad (3)$$

with  $A = -1.03 \times 10^{-2}$ ,  $B = 8.6 \times 10^{-2}$ , and  $C = 3.6 \times 10^{-2}$  to the median of the  $\sigma_{\text{sys}}$  versus  $V_{\text{mean}}$  distribution. The polynomial smoothly joins to 0.02 mag at  $V = 13$  mag. To correct the errors in the light curves, we replace the formal magnitude errors by using equation 2 and either equation 3 or 0.02 mag for  $\sigma_{\text{sys}}$ .

We also identified a systematic issue that affects the light curves of certain sources due to malfunctioning shutters. The shutters in the ASAS-SN cameras periodically start to fail. Degraded shutters do not close completely, and stray light from neighboring bright sources can impart trails on the images during readout (Figure 3). This systematic is illustrated in the light curve for the non-variable source J072955.48-521556.8 (Figure 3). We see that after the malfunctioning shutter is replaced, the light curve returns to

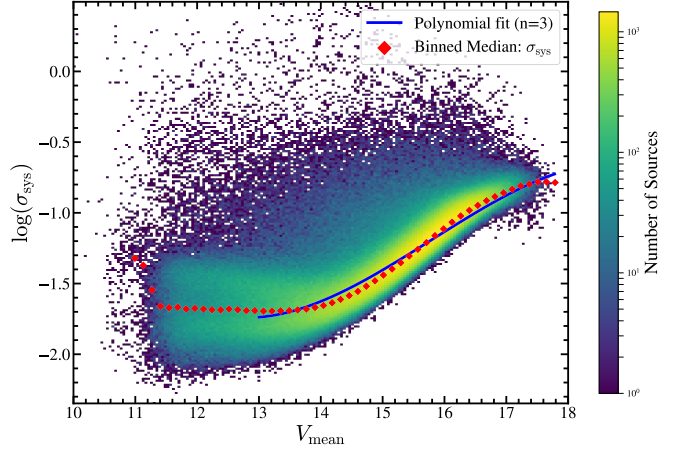


**Figure 2.** The distribution of  $\sigma_{\text{sys}}$  for the  $\sim 1.3\text{M}$  sources. The red points are the binned median values of  $\sigma_{\text{sys}}$  for this sample in bins of  $\sim 0.25$  mag. The blue curve shows a third order polynomial model for sources with  $V > 13$  mag (Equation 3).

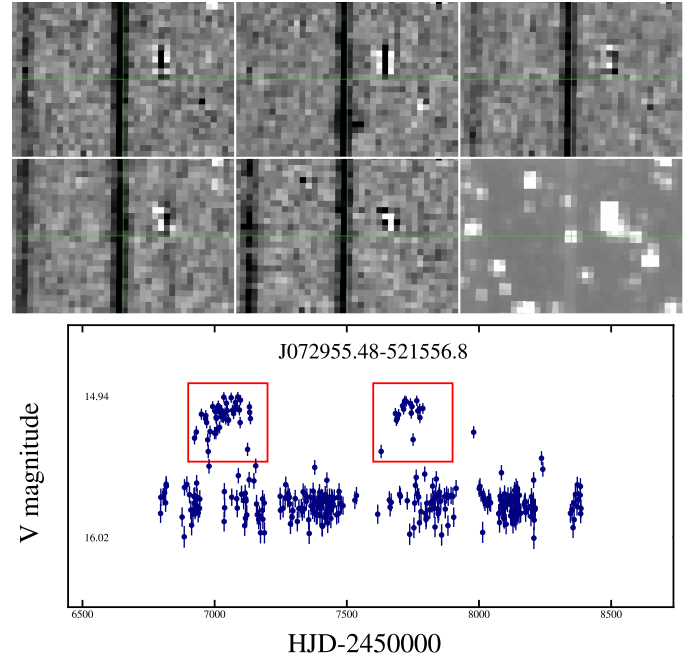


**Figure 3.** *Top:* Examples of images that are affected by a malfunctioning shutter for the non-variable source J072955.48-521556.8, with the reference image shown in the bottom right, *bottom:* The light curve for the source J072955.48-521556.8 with the affected epochs highlighted by the red boxes.

normal, but after  $\sim 700$  days, the shutter begins to fail again. Some fraction of our ASAS-SN light curves will be affected by this systematic.

### 3 VARIABILITY ANALYSIS

Here we describe the procedure we used to identify and characterize variables in the source list. We describe how we

cross-matched the APASS sources to external catalogues in Section §3.1. In Section §3.2, we describe the procedure we took to identify candidate variable sources. In Section §3.3, we discuss the application of the V2 random forest classifier model from Jayasinghe et al. (2018b) to classify these variables, and in Section §3.4, we discuss the corrections done to mitigate the effects of blending on the candidate variables.

### 3.1 Cross-matches to external catalogs

We identify cross-matches to the APASS sources with Gaia DR2 (Gaia Collaboration et al. 2018a) using the pre-computed cross matches from Marrese et al. (2018). The sources were also cross-matched to the probabilistic distance estimates from Bailer-Jones et al. (2018). We also crossmatch the sources with 2MASS (Skrutskie et al. 2006) and AllWISE (Cutri et al. 2013; Wright et al. 2010) using a matching radius of  $10''.0$ . We used TOPCAT (Taylor 2005) to cross-match the APASS sources with the 2MASS and AllWISE catalogs.

The Large Magellanic Cloud (LMC) lies within the TESS southern CVZ. We used Gaia DR2 (Gaia Collaboration et al. 2018c) to identify  $\sim 119,000$  sources from our source list that are LMC members. For sources in the LMC, we use a distance of  $d = 49.97$  kpc (Pietrzyński et al. 2013) in our variability classifier.

### 3.2 Variability cutoffs

There are numerous methods to identify variable sources from a sample of light curves. The most commonly used method involves correlating the variations observed in multiple bands to pick out ‘true’ variables from the false positives (Stetson 1996). The ASAS-SN observations used in this work are made with a single filter, which makes the use of multi-band variability statistics impossible. In this work, we used several methods, including periodogram statistics, light curve features and external photometry to identify variable sources.

We used the `astropy` implementation of the Generalized Lomb-Scargle (GLS, Zechmeister & Kürster 2009; Scargle 1982) periodogram to search for periodicity over the range  $0.05 \leq P \leq 1000$  days for each of the  $\sim 1.3M$  sources. We utilize the false alarm probability (FAP) and the power of the best GLS period as means of identifying significantly periodic sources. Sources with  $\log(\text{FAP}) < -10$  and GLS Power  $> 0.25$  were selected for further analysis (Figure 4).

We calculated the Lafler-Kinmann (Lafler & Kinman 1965; Clarke 2002) string length statistic  $T(t)$  on the temporal light curve using the definition

$$T(t) = \frac{\sum_{i=1}^N (m_{i+1} - m_i)^2}{\sum_{i=1}^N (m_i - \bar{m})^2} \times \frac{(N-1)}{2N} \quad (4)$$

from Clarke (2002), where the  $m_i$  are the magnitudes sorted temporally and  $\bar{m}$  is the mean magnitude. We can also calculate this statistic sorting the light curve based on phase for a given period, which we will call  $T(\phi|P)$ . To identify red variables, we empirically isolate sources with  $T(t) < 0.75$  and the Gaia DR2 color  $G_{BP} - G_{RP} > 1.5$  mag (Figure 5). Red

variables typically have long periods that result in noticeable structure in their temporal light curves. This structure results in smaller values of  $T(t)$  for the light curves of long period variables when compared to sources with short term variability (see Jayasinghe et al. 2018b).

We also compute the ratio of magnitudes brighter or fainter than average ( $A_{\text{HL}}$ ; Kim & Bailer-Jones 2016; Jayasinghe et al. 2018b) for all the sources. We found in Paper II that eclipsing binaries have larger values of  $A_{\text{HL}}$  than most variables, so we flag sources with  $A_{\text{HL}} > 1.5$  for further analysis. This variability cut is expected to improve the identification of detached eclipsing binaries. We also identify sources with a light curve RMS larger than the 95<sup>th</sup> percentile for the other stars in magnitude bins of 0.25 mag (Figure 6) in order to select sources with significant flux variations.

The variability cuts and the number of variable candidates isolated through each cut are summarized in Table 1. The combination of these cuts help identify different variable sources and increase our completeness when compared to relying on just one or two parameters. Through these variability cutoffs, we identified  $\sim 60,000$  unique candidates. This amounts to  $\sim 5\%$  of the sources on the initial list.

### 3.3 Variability Classification

We derived periods for the  $\sim 60,000$  variable candidates following the procedure described in Jayasinghe et al. (2018a,b). The `astrobase` implementation (Bhatti et al. 2018) of the Generalized Lomb-Scargle (GLS, Zechmeister & Kürster 2009; Scargle 1982), the Multi-Harmonic Analysis Of Variance (MHAOV, Schwarzenberg-Czerny 1996), and the Box Least Squares (BLS, Kovács et al. 2002) periodograms were used to search for periodicity in these light curves. For each periodic source, we calculate the improvement in the Lafler-Kinmann string length statistic when phased with the best period ( $T(\phi|P)$ ) when compared to the string length statistic calculated on the temporal light curve ( $T(t)$ ),

$$\delta = \frac{T(\phi|P) - T(t)}{T(t)}. \quad (5)$$

Following the period search, we use the variability classifier implemented in Jayasinghe et al. (2018b) to classify these variable candidates. We choose to visually review the classifications in order to improve our catalog. For the visual review, we select the sources with periods  $P < 40$  d if  $\delta > 0.05$  AND  $T(t) < 0.75$ . The majority of the periodic variables within this period range should show significant improvements in the string length statistic when phased with a period. Sources with  $P > 40$  d are selected if they have  $T(t) < 1$ . All irregular and aperiodic sources are also selected for visual review. In total, we visually reviewed  $\sim 23,000$  variable candidates. During the process of visual review, we identified incorrect classifications (3%) and periods (4%) and corrected them. Sources with significant systematic and spurious variability were removed (46%). We also changed the classifications of  $\sim 1300$  (6%) sources to the generic variability type (‘VAR’). At this stage, our list of variables consisted of  $\sim 12,300$  sources. This means that our initial candidate list had a false positive rate of  $\sim 80\%$ . Part of this is that we were deliberately generous in our initial selection so that we can use the results to improve this aspect of the pipeline as we

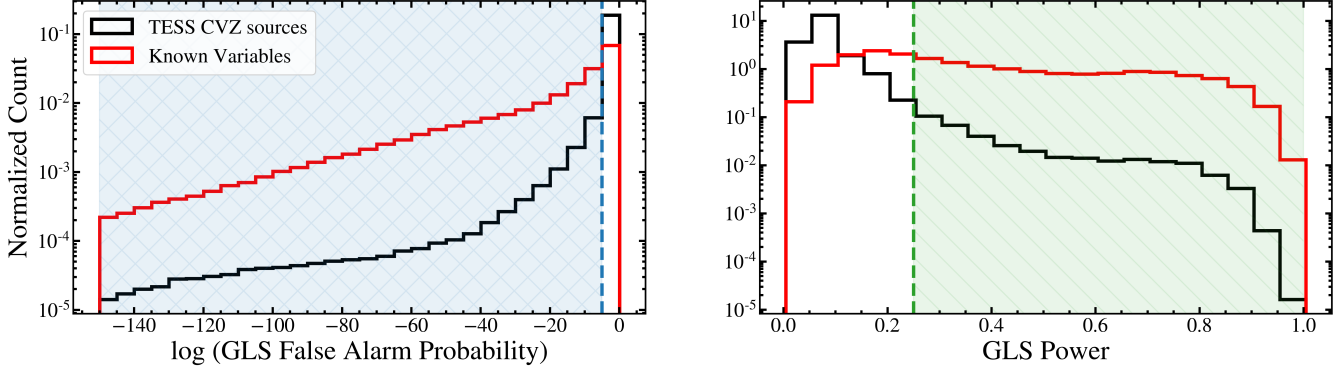


**Figure 4.** The distribution of the GLS false alarm probability (left), and the distribution of GLS power (right) for the  $\sim 1.3M$  sources (black) and the set of known variables from Jayasinghe et al. (2018b) (red). Variable candidates had to lie in the shaded regions with  $\log(\text{FAP}) < -10$  and GLS Power  $> 0.25$ .

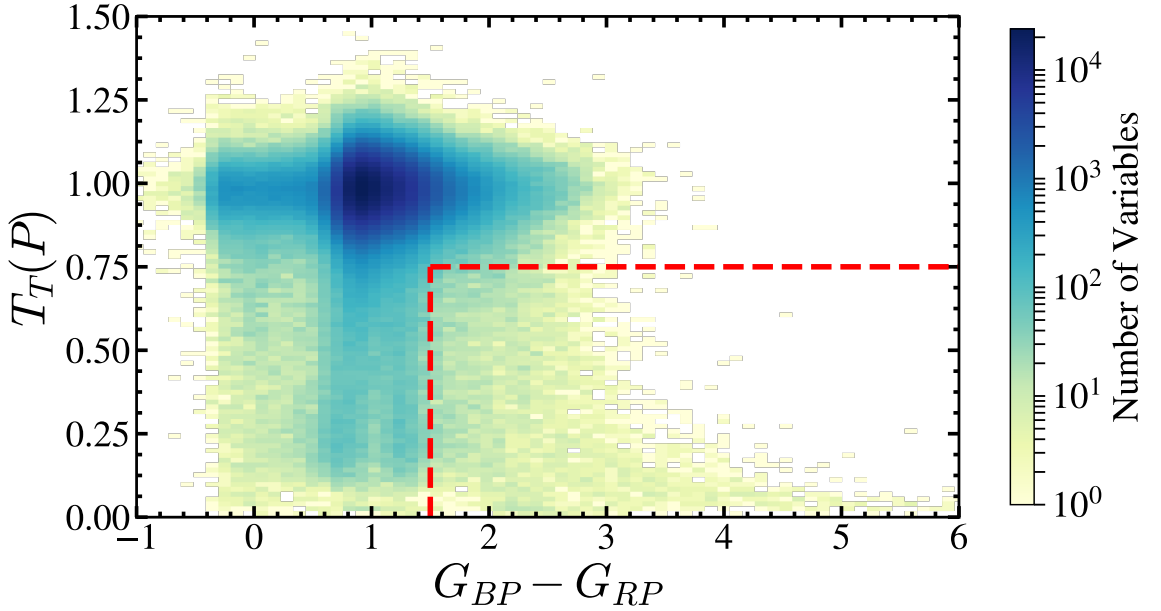


**Figure 5.** The distribution of  $G_{BP} - G_{RP}$  with  $T(t)$  for the  $\sim 1.3M$  sources. The red shaded box encloses the sources that meet the criteria of  $T(t) < 0.75$  and  $G_{BP} - G_{RP} > 1.5$  mag used to identify red variable sources.

**Table 1.** Summary of the variability selection cuts

Variable(s)	Cut	Used to identify	Sources
GLS Power	$> 0.25$	Periodic Variables	24257
GLS log (FAP)	$< -10$	Periodic Variables	39761
$G_{BP} - G_{RP}$ and $T(t)$	$> 1.5$ AND $< 0.75$	Red Variables	7741
$A_{HL}$	$> 1.5$	Eclipsing Binaries	20864
$\log(\text{RMS})$	$> 95^{\text{th}}$ percentile	Large variations	45486

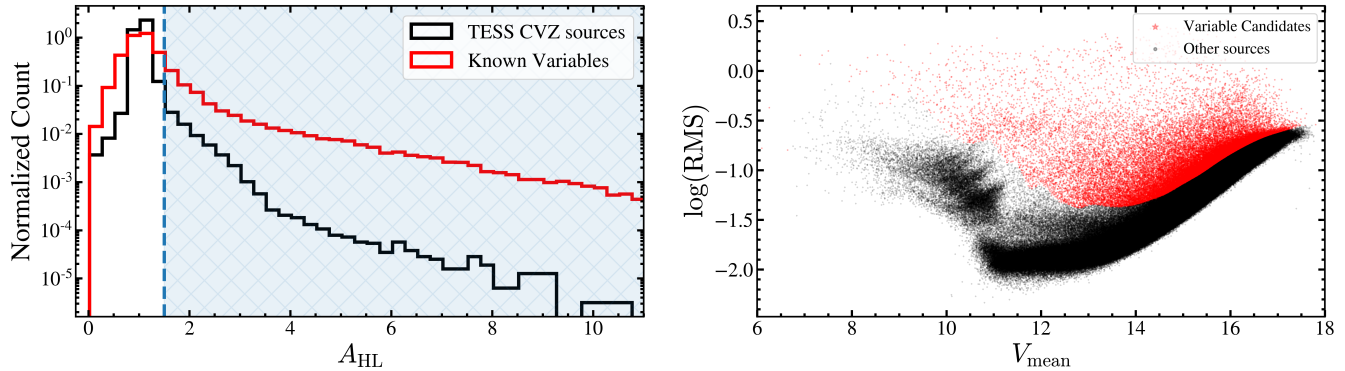


**Figure 6.** The distribution of  $A_{\text{HL}}$  (left), and the distribution of  $\log \text{RMS}$  with mean magnitude (right) for the  $\sim 1.3\text{M}$  sources. The sources with  $A_{\text{HL}} > 1.5$  are shaded in blue and the sources with  $\log \text{RMS} > 95^{\text{th}}$  percentile in each magnitude bin are shaded in red. The distribution of  $A_{\text{HL}}$  for the set of known variables from Jayasinghe et al. (2018b) is plotted in red.

progress with our effort to identify variable sources over the full sky.

### 3.4 Blending Corrections

The large pixel scale of the ASAS-SN images ( $8.^{\circ}0$ ) and the FWHM ( $\sim 16.^{\circ}0$ ) results in blending towards crowded regions. The APASS catalog was constructed with images that have a significantly smaller pixel scale ( $2.^{\circ}6$ ), and as a result of this, multiple APASS sources can fall into a single ASAS-SN pixel. We do not correct for the contaminating light in the photometry of the blended sources, but we identify and correct blended variable groups in our catalog.

Since we extracted light curves for the positions of APASS sources, we can have two or more such sources inside a single ASAS-SN resolution element. If we select the sources with another APASS neighbor within  $30.^{\circ}0$ , we find that 559 of the  $\sim 12,300$  variables had a neighbor within  $30.^{\circ}0$ . We compute the flux variability amplitudes for these sources using a random forest regression model (Jayasinghe et al. 2018b). The majority of the variable groups consisted of two sources, with a few groups consisting of up to three sources. For each variable group, we consider the source with the largest flux variability as the ‘true’ variable, and remove the other overlapping sources from the final list. Following this treatment, our list of variables consisted of  $\sim 11,700$  sources.

## 4 RESULTS

The complete catalog of  $\sim 11,700$  variables is available at the ASAS-SN Variable Stars Database (<https://asas-sn.osu.edu/variables>) along with the V-band light curves for each source. Table 2 lists the number of sources of each variability type in the catalog.

In paper II, we used the reddening-free Wesenheit magnitudes (Madore 1982; Lebzelter et al. 2018)

$$W_{\text{RP}} = M_{\text{G}_{\text{RP}}} - 1.3(G_{\text{BP}} - G_{\text{RP}}), \quad (6)$$

and

$$W_{\text{JK}} = M_{\text{K}_s} - 0.686(J - K_s) \quad (7)$$

for variability classification. The Wesenheit  $W_{\text{RP}}$  vs.  $G_{\text{BP}}$  –

$G_{\text{RP}}$  color-magnitude diagram for all the variables is shown in Figure 7. We have sorted the variables into groups to highlight the different classes of variable sources. Owing to the magnitude limit of ASAS-SN, we are only able to detect sufficiently bright sources ( $V \lesssim 16$  mag,  $W_{\text{RP}} \lesssim 1.5$  mag) in the LMC. This is evident in the Wesenheit color-magnitude diagram for the LMC sources. For the sources outside the LMC, we probe a wider range of magnitudes ( $W_{\text{RP}} \lesssim 6$  mag), including RR Lyrae, rotational variables and  $\delta$  Scuti variables.

We have also plotted the Wesenheit  $W_{\text{RP}}$  vs.  $G_{\text{BP}} - G_{\text{RP}}$  color-magnitude diagram for all the periodic variables in Figure 8, with the points colored according to the period. This essentially highlights the large dynamic range in period probed by the ASAS-SN light curves.

We note that the identification of Mira variables in the LMC is hindered by blending. Due to blended light, the observed ASAS-SN amplitudes of these sources fall below the amplitude threshold of  $V > 2$  mag that is used to define a Mira variable in our pipeline. In reality, some fraction of the LMC semi-regular variables in this catalog are actually Mira variables. From the sample of known semi-regular variables in the LMC, we estimate that the fraction of Mira variables classified as semi-regular variables is  $\sim 23\%$ .

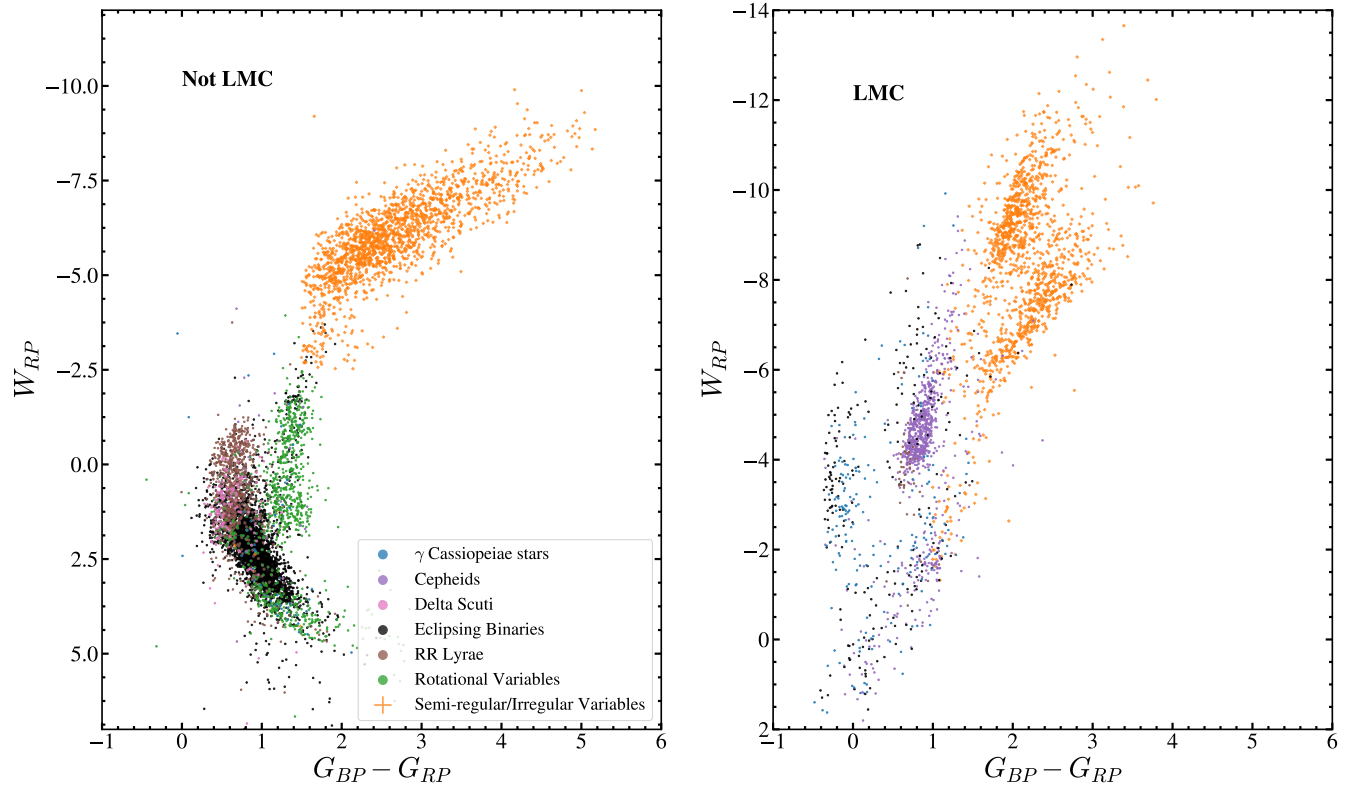
Using the same color scheme, the combined Wesenheit  $W_{\text{JK}}$  PLR diagram for the periodic variables is shown in Figure 9. The PLR sequences for the Cepheids and semi-regular variables in the LMC are well defined (Soszynski et al. 2005). Most of the eclipsing binaries identified in the LMC are either detached or semi-detached systems, and do not follow the well defined PLR for contact binaries that is observed in the PLR diagram for the sources outside the LMC.

We also show the sky distribution of the variables identified in this work in Figure 10. We see that the distribution of eclipsing binaries and rotational variables (black points) is random, but the distribution of Cepheids is strongly clustered towards the LMC as is expected. We also note the clustering of semi-regular/irregular variables (red giants) towards the LMC and the Galactic disk.

We matched our list of variables to the VSX (Watson et al. 2006) catalog available in October 2018, with a matching radius of  $16.^{\circ}0$  to identify previously discovered variables.

**Table 2.** Variables by type

VSX Type	Description	LMC	Not LMC	New discoveries
CWA	W Virginis type variables with $P > 8$ d	10	–	1
CWB	W Virginis type variables with $P < 8$ d	4	8	2
DCEP	Fundamental mode Classical Cepheids	577	12	12
DCEPS	First overtone Cepheids	280	9	10
DSCT	$\delta$ Scuti variables	–	44	42
EA	Detached Algol-type binaries	103	1109	865
EB	$\beta$ Lyrae-type binaries	129	523	353
EW	W Ursae Majoris type binaries	97	1961	1228
ELL	Ellipsoidal Variables	1	11	12
HADS	High amplitude $\delta$ Scuti variables	–	102	61
ROT	Rotational variables	–	881	813
RRAB	RR Lyrae variables (Type ab)	42	444	44
RRC	First Overtone RR Lyrae variables	4	443	217
RRD	Double Mode RR Lyrae variables	–	4	3
RVA	RV Tauri variables (Subtype A)	9	1	1
SR	Semi-regular variables	1017	1487	1340
L	Irregular variables	298	137	262
GCAS	$\gamma$ Cassiopeiae variables	191	49	128
YSO	Young stellar objects	2	8	6
ROT:	Uncertain rotational variables	–	186	174
DSCT:	Uncertain $\delta$ Scuti variables	4	63	48
GCAS:	Uncertain $\gamma$ Cassiopeiae variables	10	–	3
VAR	Generic variables	40	1390	1385

**Figure 7.** The Wesenheit  $W_{RP}$  vs.  $G_{BP} - G_{RP}$  color-magnitude diagram for the variables, outside the LMC (left), and in the LMC (right).

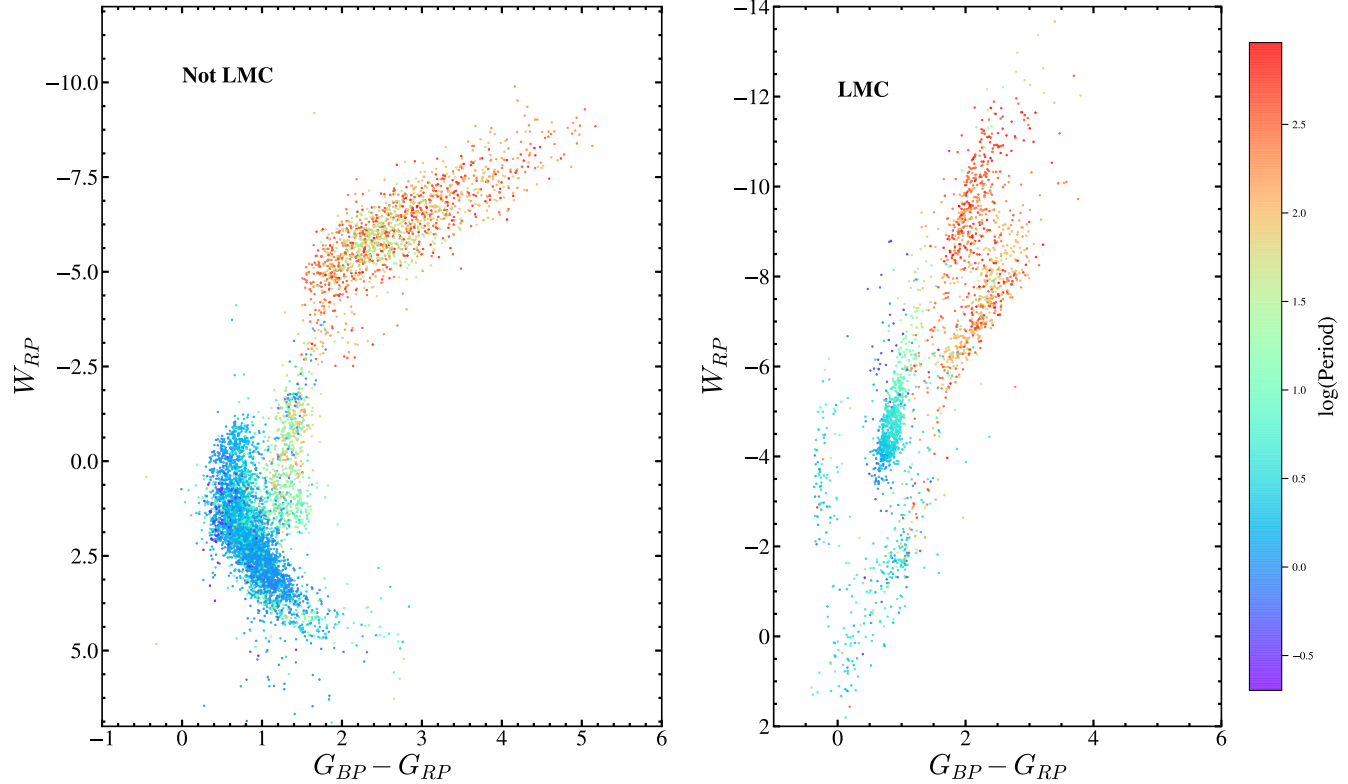


**Figure 8.** The Wesenheit  $W_{RP}$  vs.  $G_{BP} - G_{RP}$  color-magnitude diagram for the periodic variables, outside the LMC (left), and in the LMC (right). The points are colored by the period.

The variables discovered by the All-Sky Automated Survey (ASAS; Pojmanski 2002) and the Catalina Real-Time Transient Survey (CRTS; Drake et al. 2014) are included in the VSX database. We also match our variables to the catalogs of variable stars discovered by ASAS-SN (Jayasinghe et al. 2018a), the catalogs of variable stars in the Magellanic clouds and the Galactic bulge from the Optical Gravitational Lensing Experiment (OGLE; Udalski 2003; Pawlak et al. 2016; Soszyński et al. 2016, and references therein), the Gaia DR2 catalog of variables (Gaia Collaboration et al. 2018a; Holl et al. 2018; Gaia Collaboration et al. 2018b), the catalog of variables from the Asteroid Terrestrial-impact Last Alert System (ATLAS; Tonry et al. 2018; Heinze et al. 2018), the catalog of KELT variables (Oelkers et al. 2018) and the variables from MACHO (Alcock et al. 1997). Of the  $\sim 11,700$  variables identified in this work,  $\sim 4,700$  were previously discovered by other surveys, as also listed in Table 2. The majority of these known variables consist of eclipsing binaries ( $\sim 31\%$ ), irregular/semi-regular variables ( $\sim 28\%$ ) and Cepheids ( $\sim 19\%$ ).

This leaves  $\sim 7,000$  new variables. Most of the new discoveries are eclipsing binaries ( $\sim 35\%$ ) and irregular/semi-regular variables ( $\sim 23\%$ ). We also discovered 128 new GCAS variables, 81 of which are located in the LMC. GCAS variables are rapidly rotating, early-type irregular variable stars (typically Be stars) with mass outflow from their equatorial regions. Example light curves for the newly identified GCAS variables are shown in Figure 12.

We also discovered another long period detached eclips-

ing binary (ASASSN-V J080709.46-591028.3) in this work. ASASSN-V J080709.46-591028.3 is located away from the LMC and has an orbital period of  $P_{\text{orb}} \sim 682$  d ( $\sim 1.9$  yr). Its light curve shows evidence of both a primary and secondary eclipse with a primary eclipse depth of  $\sim 1$  mag (Figure 11).

A non-negligible fraction of these new discoveries were classified as generic variables ( $\sim 20\%$ ). These are mostly low amplitude or faint sources. Example light curves are shown for a subset of the newly discovered periodic (irregular) variables in Figure 9 (10).

## 5 CONCLUSIONS

We systematically searched for variable sources in a  $\sim 1000 \text{ deg}^2$  region surrounding the Southern ecliptic pole. This region is coincident with the Southern continuous viewing zone for the TESS satellite and thus, a large majority of these sources will have excellent TESS light curves.

Through our search, we identified  $\sim 11,700$  variable sources, of which  $\sim 7,000$  are new discoveries. Variable sources identified in the LMC largely consist of luminous variables, including Cepheids, GCAS variables (Be stars) and red giants. We identify a broader sample of variables outside the LMC, including RR Lyrae, eclipsing binaries, rotational variables and  $\delta$  Scuti variables.

We have developed a user friendly interface to retrieve pre-computed ASAS-SN V-band light curves for APASS sources. The V-band light curves of all the  $\sim 1.3$  M

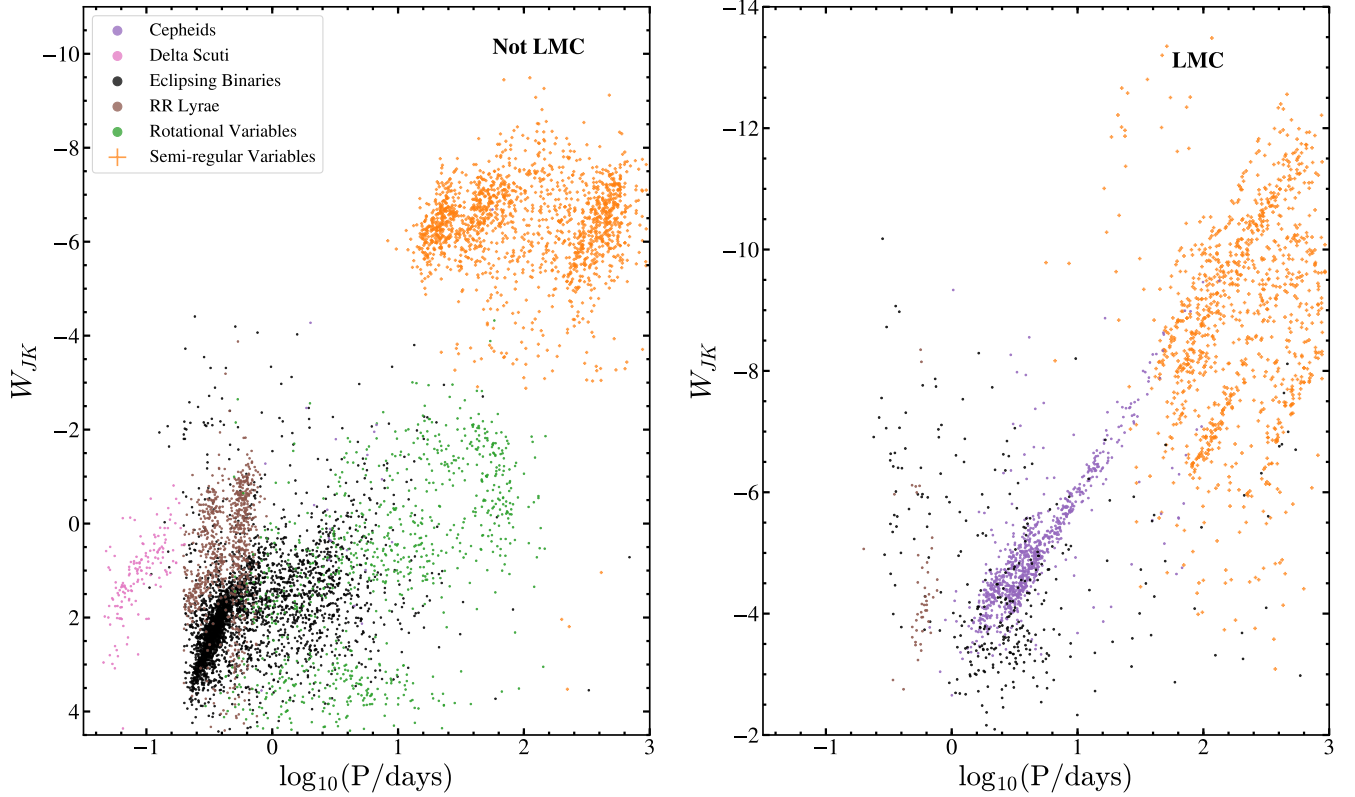


**Figure 9.** The Wesenheit  $W_{JK}$  PLR diagram for the periodic variables, outside the LMC (left), and in the LMC (right). The points are colored as in Figure 7.

sources studied in this work are available online at the ASAS-SN Photometry Database (<https://asas-sn.osu.edu/photometry>). To highlight the possible blended sources, a flag is assigned to each source if the distance to the nearest APASS neighbor is  $<16''$ . The new variable sources have also been added to the ASAS-SN variable stars database (<https://asas-sn.osu.edu/variables>).

As part of our ongoing effort to systematically analyze all the  $\sim 50$  million  $V < 17$  mag APASS sources for variability, we will gradually update this database with the light curves for the sources across the remainder of the sky over the course of 2019. This work provides long baseline V-band light curves for a large fraction of the sources in the TESS southern CVZ and is a useful supplement to the short baseline TESS light curves that possess better photometric precision.

## ACKNOWLEDGEMENTS

We thank the Las Cumbres Observatory and its staff for its continuing support of the ASAS-SN project. We also thank the Ohio State University College of Arts and Sciences Technology Services for helping us set up and maintain the ASAS-SN variable stars and photometry databases.

ASAS-SN is supported by the Gordon and Betty Moore Foundation through grant GBMF5490 to the Ohio State University and NSF grant AST-1515927. Development of ASAS-SN has been supported by NSF grant AST-0908816,

the Mt. Cuba Astronomical Foundation, the Center for Cosmology and AstroParticle Physics at the Ohio State University, the Chinese Academy of Sciences South America Center for Astronomy (CAS- SACA), the Villum Foundation, and George Skestos.

This work is supported in part by Scialog Scholar grant 24215 from the Research Corporation. TAT acknowledges support from a Simons Foundation Fellowship and from an IBM Einstein Fellowship from the Institute for Advanced Study, Princeton. Support for JLP is provided in part by the Ministry of Economy, Development, and Tourism's Millennium Science Initiative through grant IC120009, awarded to The Millennium Institute of Astrophysics, MAS. SD acknowledges Project 11573003 supported by NSFC. Support for MP and OP has been provided by the PRIMUS/SCI/17 award from Charles University. This work was partly supported by NSFC 11721303.

This work has made use of data from the European Space Agency (ESA) mission *Gaia* (<https://www.cosmos.esa.int/gaia>), processed by the *Gaia* Data Processing and Analysis Consortium. This publication makes use of data products from the Two Micron All Sky Survey, as well as data products from the Wide-field Infrared Survey Explorer. This research was also made possible through the use of the AAVSO Photometric All-Sky Survey (APASS), funded by the Robert Martin Ayers Sciences Fund.

This research has made use of the VizieR catalogue access tool, CDS, Strasbourg, France. This research made

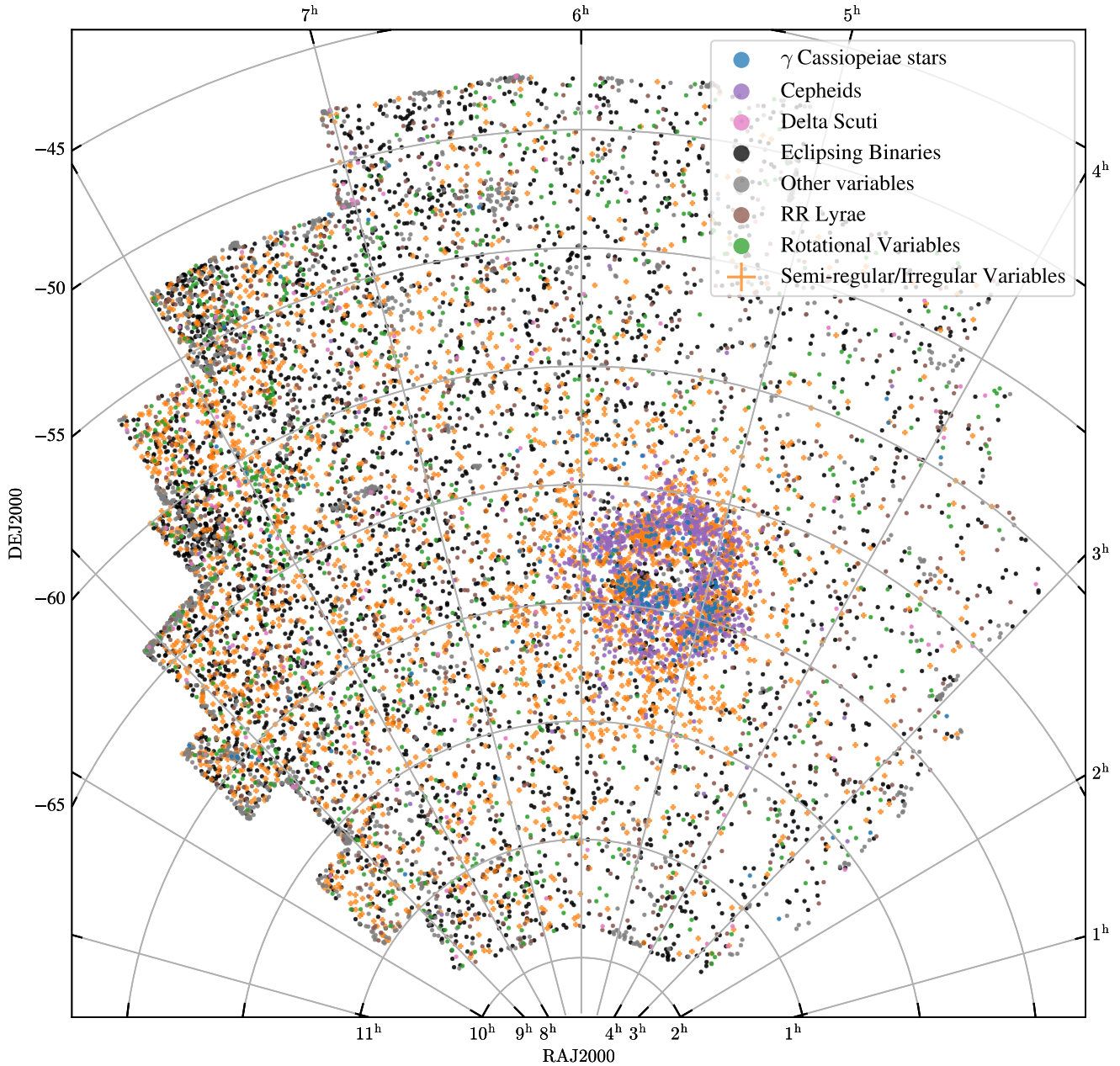


**Figure 10.** The sky distribution of the variables in equatorial coordinates. The points are colored as in Figure 7.

ualso se of Astropy, a community-developed core Python package for Astronomy (Astropy Collaboration, 2013).

## REFERENCES

- Alard, C. 2000, *A&AS*, 144, 363  
 Alard, C., & Lupton, R. H. 1998, *ApJ*, 503, 325  
 Alcock, C., Allsman, R. A., Alves, D., et al. 1997, *ApJ*, 486, 697  
 Astropy Collaboration, Robitaille, T. P., Tollerud, E. J., et al. 2013, *A&A*, 558, A33  
 Bailer-Jones, C. A. L., Rybizki, J., Fouesneau, M., Mantelet, G., & Andrae, R. 2018, *AJ*, 156, 58  
 Beaton, R. L., Bono, G., Braga, V. F., et al. 2018, *Space Sci. Rev.*, 214, 113  
 Bhatti, W., Bouma, L. G., Wallace, J., et al. 2018, *astrobase*, v0.3.8, Zenodo, <http://doi.org/10.5281/zenodo.1185231>  
 Brown, T. M., Baliber, N., Bianco, F. B., et al. 2013, *PASP*, 125, 1031  
 Brown, J. S., Stanek, K. Z., Holoi, T. W.-S., et al. 2018, *arXiv:1810.00011*  
 Clarke, D. 2002, *A&A*, 386, 763  
 Cutri, R. M., & et al. 2013, *VizieR Online Data Catalog*, 2328, 149  
 Derue, F., Marquette, J.-B., Lupone, S., et al. 2002, *A&A*, 389, 149  
 Drake, A. J., Graham, M. J., Djorgovski, S. G., et al. 2014, *ApJS*, 213, 9

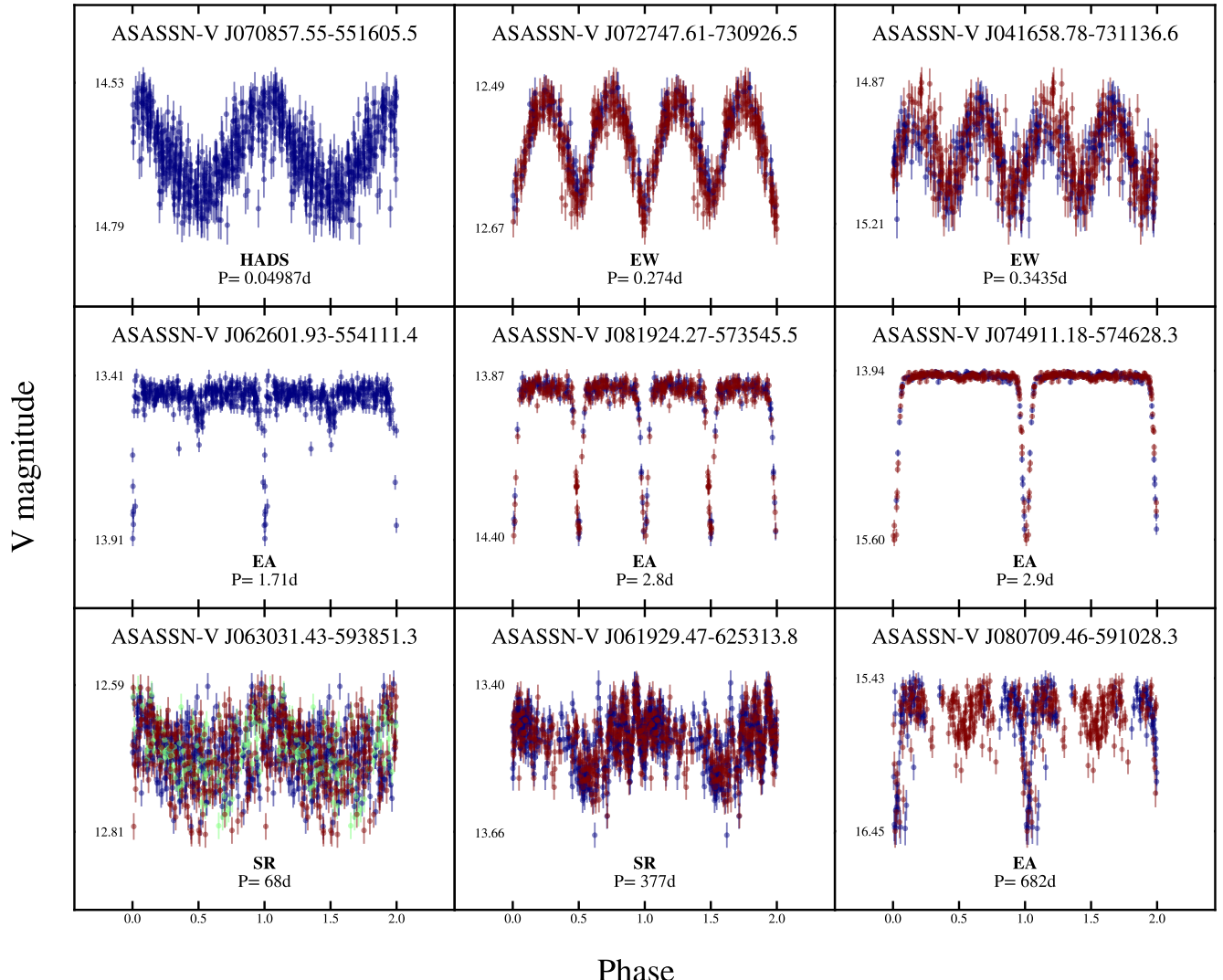


**Figure 11.** Phased light curves for examples of the newly discovered periodic variables. The light curves are scaled by their minimum and maximum V-band magnitudes. Different colored points correspond to data from the different ASAS-SN cameras. The different variability types are defined in Table 2.

- Feast, M., & Whitelock, P. A. 2014, *Setting the Scene for Gaia and LAMOST*, 40.
- Gaia Collaboration, Brown, A. G. A., Vallenari, A., et al. 2018, arXiv:1804.09365
- Gaia Collaboration, Eyer, L., Rimoldini, L., et al. 2018, arXiv:1804.09382
- Gaia Collaboration, Helmi, A., van Leeuwen, F., et al. 2018, *A&A*, 616, A12.
- Heinze, A. N., Tonry, J. L., Denneau, L., et al. 2018, arXiv:1804.02132
- Henden, A. A., Levine, S., Terrell, D., & Welch, D. L. 2015, *American Astronomical Society Meeting Abstracts* #225, 225, 336.16
- Holl, B., Audard, M., Nienartowicz, K., et al. 2018, arXiv:1804.09373
- Holtzman, J. A., Shetrone, M., Johnson, J. A., et al. 2015, *AJ*, 150, 148
- Holoiien, T. W.-S., Prieto, J. L., Bersier, D., et al. 2014, *MNRAS*, 445, 3263
- Holoiien, T. W.-S., Kochanek, C. S., Prieto, J. L., et al. 2016, *MNRAS*, 455, 2918
- Holoiien, T. W.-S., Brown, J. S., Stanek, K. Z., et al. 2017, *MNRAS*, 471, 4966
- Holoiien, T. W.-S., Brown, J. S., Valley, P. J., et al. 2018, arXiv:1811.08904
- Holoiien, T. W.-S., Huber, M. E., Shappee, B. J., et al. 2018, arXiv:1808.02890
- Jayasinghe, T., Kochanek, C. S., Stanek, K. Z., et al. 2018, *MNRAS*, 477, 3145
- Jayasinghe, T., Stanek, K. Z., Kochanek, C. S., et al. 2018, arXiv:1809.07329
- Jayasinghe, T., Stanek, K. Z., Kochanek, C. S., et al. 2018, *Research Notes of the American Astronomical Society*, 2, 181
- Jayasinghe, T., Stanek, K. Z., Kochanek, C. S., et al. 2018, *Research Notes of the American Astronomical Society*, 2, 125
- Kim, D.-W., & Bailer-Jones, C. A. L. 2016, *A&A*, 587, A18
- Kochanek, C. S., Shappee, B. J., Stanek, K. Z., et al. 2017, *PASP*, 129, 104502
- Kovács, G., Zucker, S., & Mazeh, T. 2002, *A&A*, 391, 369
- Lafler, J., & Kinman, T. D. 1965, *ApJS*, 11, 216

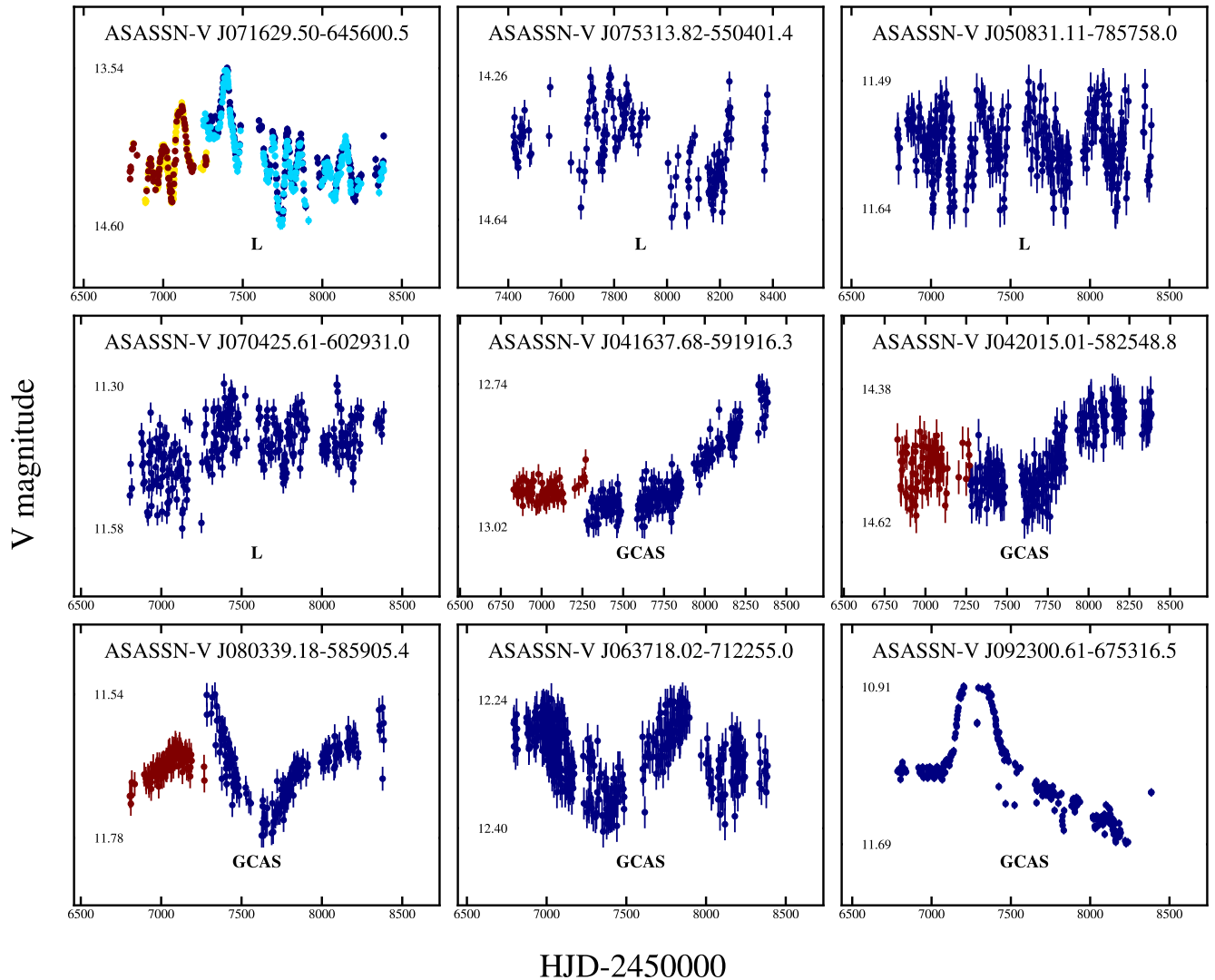


**Figure 12.** Light curves for examples of the newly discovered irregular variables. The format is the same as for Fig. 11

- Lebzelter, T., Mowlavi, N., Marigo, P., et al. 2018, arXiv:1808.03659
- Leavitt, H. S. 1908, Annals of Harvard College Observatory, 60, 87
- Madore, B. F. 1982, ApJ, 253, 575
- Marrese, P. M., Marinoni, S., Fabrizio, M., & Altavilla, G. 2018, arXiv:1808.09151
- Matsunaga, N. 2018, Rediscovering Our Galaxy, 57.
- Matsunaga, N., Fukushi, H., Nakada, Y., et al. 2006, MNRAS, 370, 1979
- Oelkers, R. J., Rodriguez, J. E., Stassun, K. G., et al. 2018, AJ, 155, 39
- Pawlak, M., Soszyński, I., Udalski, A., et al. 2016, Acta Astron., 66, 421
- Pietrzyński, G., Graczyk, D., Gieren, W., et al. 2013, Nature, 495, 76
- Pojmanski, G. 2002, Acta Astron., 52, 397
- Ricker, G. R., Winn, J. N., Vanderspek, R., et al. 2015, Journal of Astronomical Telescopes, Instruments, and Systems, 1, 014003
- Rodríguez, R., Schmidt, S. J., Jayasinghe, T., et al. 2018, Research Notes of the American Astronomical Society, 2, 8

- Scargle, J. D. 1982, ApJ, 263, 835
- Schmidt, S. J., Shappee, B. J., van Saders, J. L., et al. 2018, arXiv:1809.04510
- Schwarzenberg-Czerny, A. 1996, ApJ, 460, L107
- Shappee, B. J., Prieto, J. L., Grupe, D., et al. 2014, ApJ, 788, 48
- Shields, J. V., Jayasinghe, T., Stanek, K. Z., et al. 2018, arXiv:1809.04075
- Skrutskie, M. F., Cutri, R. M., Stiening, R., et al. 2006, AJ, 131, 1163
- Soszynski, I., Udalski, A., Kubiak, M., et al. 2005, Acta Astron., 55, 331.
- Soszyński, I., Pawlak, M., Pietrukowicz, P., et al. 2016, Acta Astron., 66, 405
- Stassun, K. G., Oelkers, R. J., Pepper, J., et al. 2018, AJ, 156, 102
- Stetson, P. B. 1996, PASP, 108, 851
- Taylor, M. B. 2005, Astronomical Data Analysis Software and Systems XIV, 347, 29
- Thompson, T. A., Kochanek, C. S., Stanek, K. Z., et al. 2018, arXiv:1806.02751
- Tony, J. L., Denneau, L., Heinze, A. N., et al. 2018, PASP, 130, 064505

- Torres, G., Andersen, J., & Giménez, A. 2010, A&ARv, 18, 67  
Tucker, M. A., Shappee, B. J., Holoiu, T. W.-S., et al. 2018,  
arXiv:1808.07875  
Udalski, A. 2003, Acta Astron., 53, 291  
Watson, C. L., Henden, A. A., & Price, A. 2006, Society for As-  
tronomical Sciences Annual Symposium, 25, 47  
Wright, E. L., Eisenhardt, P. R. M., Mainzer, A. K., et al. 2010,  
AJ, 140, 1868  
Woźniak, P. R., Vestrand, W. T., Akerlof, C. W., et al. 2004, AJ,  
127, 2436  
Zechmeister, M., & Kürster, M. 2009, A&A, 496, 577

This paper has been typeset from a  $\text{\TeX}$ / $\text{\LaTeX}$  file prepared by  
the author.